SUPPLEMENTARY INFORMATION

A Great Earthquake Doublet and Seismic Stress Transfer Cycle in the Central Kuril Islands

Charles J. Ammon[1], Hiroo Kanamori[2] & Thorne Lay[3]

[1]Department of Geosciences, The Pennsylvania State University, 440 Deike Building, University Park, PA 16802, USA. [2]Seismological Laboratory, California Institute of Technology, MS 252-21, Pasadena, CA 91125, USA, [3]Earth and Planetary Sciences Department, University of California, Santa Cruz, CA 95064, USA.

Rupture Model Geometry and Sensitivity Analysis Results

The global centroid-moment tensor (GCMT) point-source inversion using long-period body and surface waves for the 15 November 2006 event indicates a thrusting geometry with fault strike, $\phi = 215°$, dip, $\delta = 15°$ and rake $\lambda = 92°$, with a seismic moment, M_o, of 3.5×10^{21} N-m (ref. S1). A similar geometry was obtained from centroid-moment tensor inversion of surface waves by J. Polet (personal communication, 2007), with $\phi = 206.1°$, $\delta = 9.2°$ and $\lambda = 84.3°$ and $M_o = 3.9 \times 10^{21}$ N-m. The 15 November hypocenter was fixed at 11 km based on waveform modeling estimates of near-hypocenter foreshocks. For the 13 January 2007 event, the GCMT solution indicates an oblique normal faulting geometry for a fault with $\phi = 43°$, $\delta = 59°$, and $\lambda = -115°$, or for the complementary plane with $\phi = 266°$, $\delta = 39°$ and $\lambda = -54°$, with $M_o = 1.78 \times 10^{21}$ N-m (ref. S1). The plane dipping to the southeast has a strike close to the trends of the trench and aftershock distribution, whereas the northwesterly dipping plane is more oblique to both. Polet's surface wave inversion for the 13 January 2007 event has a less oblique-slip geometry with $\phi = 48.2°$, $\delta = 50.7°$ and $\lambda = -103.1°$, or $\phi = 248.3°$, $\delta = 41.1°$, and $\lambda = -74.5°$, with $M_o = 1.4 \times 10^{21}$ N-m. Both planes in this solution are oblique to the trench and the normal faulting aftershocks. The moderate-size aftershocks with GCMT mechanism information generally have fault plane strikes that parallel the trench. The hypocenter was fixed at 22 km, but is not well resolved. We tried inversions with shallower initiation points and obtained similar results. Our choice to place the hypocenter deep in the seismogenic zone is consistent with some aftershock depths in the vicinity.

For the 15 November 2006 event, we considered fault models extending as much as 320 km along strike and 140 km down-dip from the trench. Satisfactory models were found for both the GCMT and Polet geometries. On the basis of larger aftershock depth determinations by waveform modeling, we fixed the mechanism to have the GCMT orientation. Inversions were first performed that allowed for variable rake, finding only ±5° deviations from the average rake, so we held rake constant in the final inversions. SH waves were included, but time alignments prove challenging due to the emergent nature of the waveforms, and were guided by initial P-wave-only inversions. Our final inversions included azimuthally distributed broadband P waves, SH waves and R1 Rayleigh wave STFs.

The total rupture duration was found to be about 120 s, with the slip zone extending mainly northeastward from the epicenter, based on detectable body wave and surface wave directivity. The estimated length of the rupture zone depends on the assumed rupture velocity, which is only loosely constrained by directivity analysis to be in the range from 1.5-2.5 km/s, constrained primarily by directivity effects in the Rayleigh wave pulses. The slip distribution for a rupture velocity of 2 km/s and a shear modulus of 40 GPa, along with the source moment-rate history as observed perpendicular to the fault are shown in figure S2. The moment-rate history is insensitive to assumptions about rupture speed, and robust to changes in the waveform combinations used in the inversion. Inversions with layered velocity models were performed, but the final case is for a half space with P-wave velocity of 6.7 km/s and a density of 2.9 x 10^3 Kg/m^3, with a 3 km thick water layer. The average slip is about 4.6 m. Large slip is located in two patches northeast of the hypocenter, with the overall rupture length being about 200 km. The P and SH waveforms begin gradually and are very well fit by this slip model (figure S2). The location of the large slip patches is better constrained in position along strike than along dip, but the absolute position along strike varies directly with the assumed rupture velocity. The model's seismic moment, 4.6 x 10^{21} N-m (M_w = 8.4), is somewhat larger than the GCMT seismic moment.

Finite source models for the 13 January 2007 event were obtained for the GCMT and Polet (and many other) fault geometries dipping either southeast or northwest in an effort to resolve the fault plane ambiguity. Similar slip distributions and overall waveform fits are found for either fault orientation, with concentration of slip in the upper 25 km of the oceanic lithosphere, and little constraint on rupture velocity. For lower rupture velocities near 2 km/s the estimated peak slip at crustal depths is very large (>30 m), over fault lengths of 70 to 90-km. Larger rupture velocities of up to 3.5 km/s yield estimated peak slip of 10-20 m and total rupture lengths of 120-160 km. The weak tsunami excitation tends to favor lower slip, and corresponding higher rupture velocities. The fit to P waveforms at stations to the south tends to be better for the northwest dipping plane, but stations to the east are fit better for the southeast dipping geometry (figure S3). While prescribing a strike for either plane parallel to the aftershock distribution results in a good fit to the P waves, the long-period Love and Rayleigh wave signals require some oblique slip overall, and we ultimately adopt the GCMT orientation to ensure compatibility with long-periods. While slightly better overall fits were obtained for the northwest dipping fault geometry assuming a shallow hypocenter, the GCMT orientation of this plane deviates from the trend of the aftershocks and trench. It is possible that aftershocks are an unreliable guide as to the fault geometry, given that their mechanisms deviate from the great event (figure S1), but we chose the SE dipping plane for the final model since this does have a trend compatible with the aftershocks. For this case, having the hypocenter at a depth of about 22 km gives a better solution than a shallow hypocenter. The waveform fits and slip model for our final model are shown in figure S4. The event is characterized by a large slip pulse in the upper 25 km of the fault, with a length of about 200 km. The seismic moment is 1.5 x 10^{21} N-m. The average slip is about 9.6 m over a 120 km 20 km fault extent (converting from moment to slip using a shear modulus of 52 GPa). Some weaker slip appears to extend to depths of 30-35 km, but resolution is limited. The moment rate function is dominated by a large pulse with a duration of 45-50 s, with some weak energy release during the next 20 s. This latter energy is not well accounted for by kinematic rupture models with high constant rupture velocity, but appears to come from relatively large depth (>25 km) not too far from the epicenter. Delayed, deep slip on the fault is

a tentative explanation for this energy, but more complex rupture parameterizations will need to be examined to resolve it better.

Compressional Earthquake Activity in the Outer-Rise Region

In contrast with the post-15-November initiation of extensional activity in the central Kurils outer rise region, compressional activity in the outer rise region of the central Kurils has been noted for some time, particularly in (S3). The compressional events from (S3) are identified on the map in Figure S4 by red shading in the focal mechanisms, others are included in the gray mechanisms of the GCMT catalog. The magnitude for the March 1963 event is listed as 7.7 in (S3), but is listed as 7.2 in (S4), and has an Ms of 7.2 in the USGS catalogs. Several other outer rise compressional events not in the table are located to the north, near the inferred southern end of the Great 1952 Kamchatka earthquake.

Table S1
Compressional Events in the Central Kurils Outer Rise Region

Date	Origin Time	Lat	Lon	Depth	mb	Ms	Mw	Reference
16 Mar 1963	08:44:51	46.79	154.83	10-50	7.7	7.2	-	S3
02 Dec 1971	17:18:21	44.77	153.33	38	6.2	6.3	-	S3
23 Aug 1981	12:00:26	48.71	157.37	20-42	6.0	5.8	6.0	S3/GCMT
02 Aug 1983	06:08:06	45.17	153.48	68	5.4	-	5.4	GCMT
10 Sep 1990	03:51:24	46.59	155.48	23	5.3	4.6	5.3	GCMT

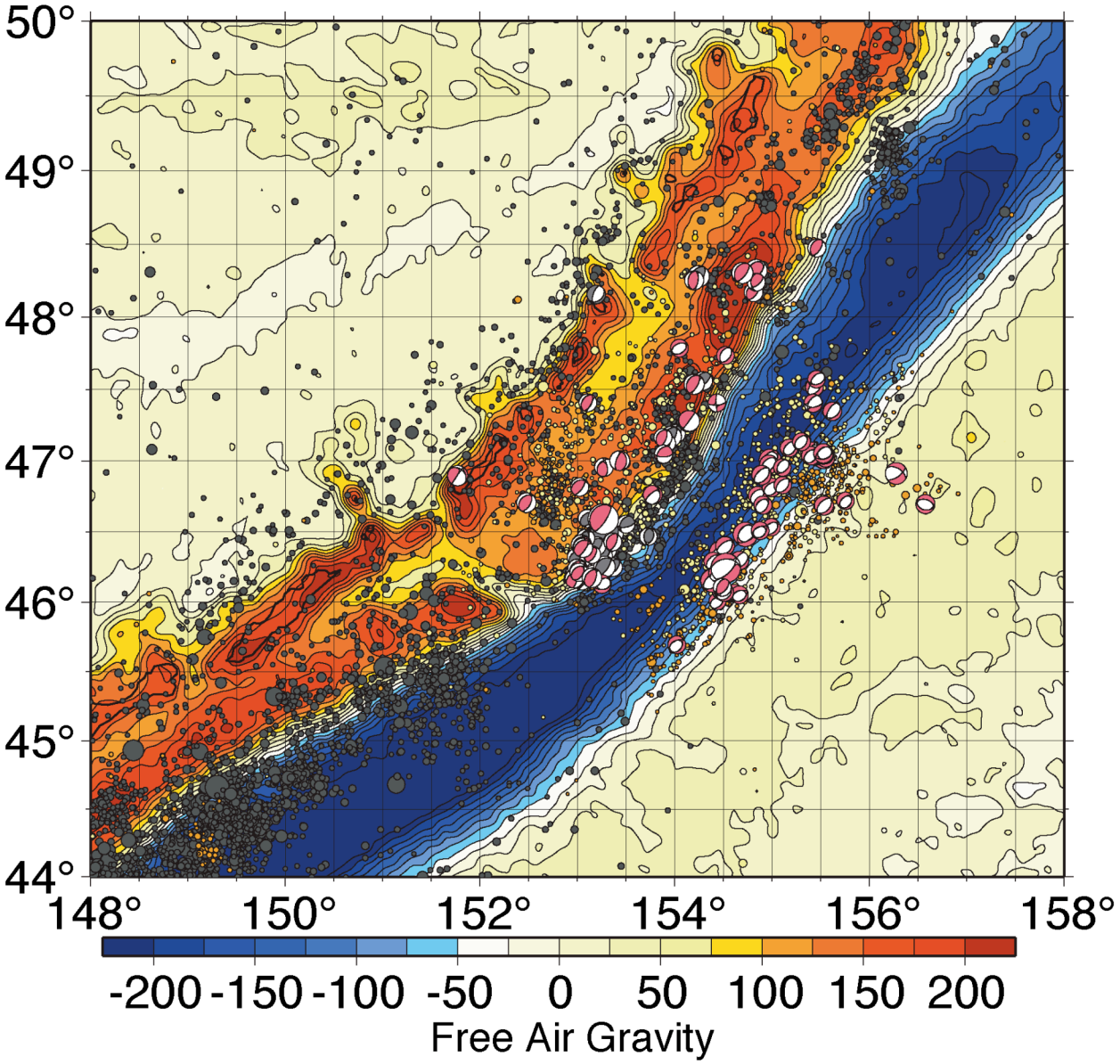

Figure S1 | Free air gravity anomalies. Map of the free air gravity anomaly along the central Kuril Island arc, superimposed by regional seismicity from the National Earthquake Information Center bulletin (gray dots, with radius scaled proportional to magnitude), and global centroid-moment tensor (GCMT) solutions for foreshocks (gray) and mainshocks/aftershocks of the great doublet (red). Note the narrowing of the trench gravitational signal in the vicinity of the double sequence and the fact that this appears to largely stem from broadening of the fore-arc rather than seaward disruption of the trench.

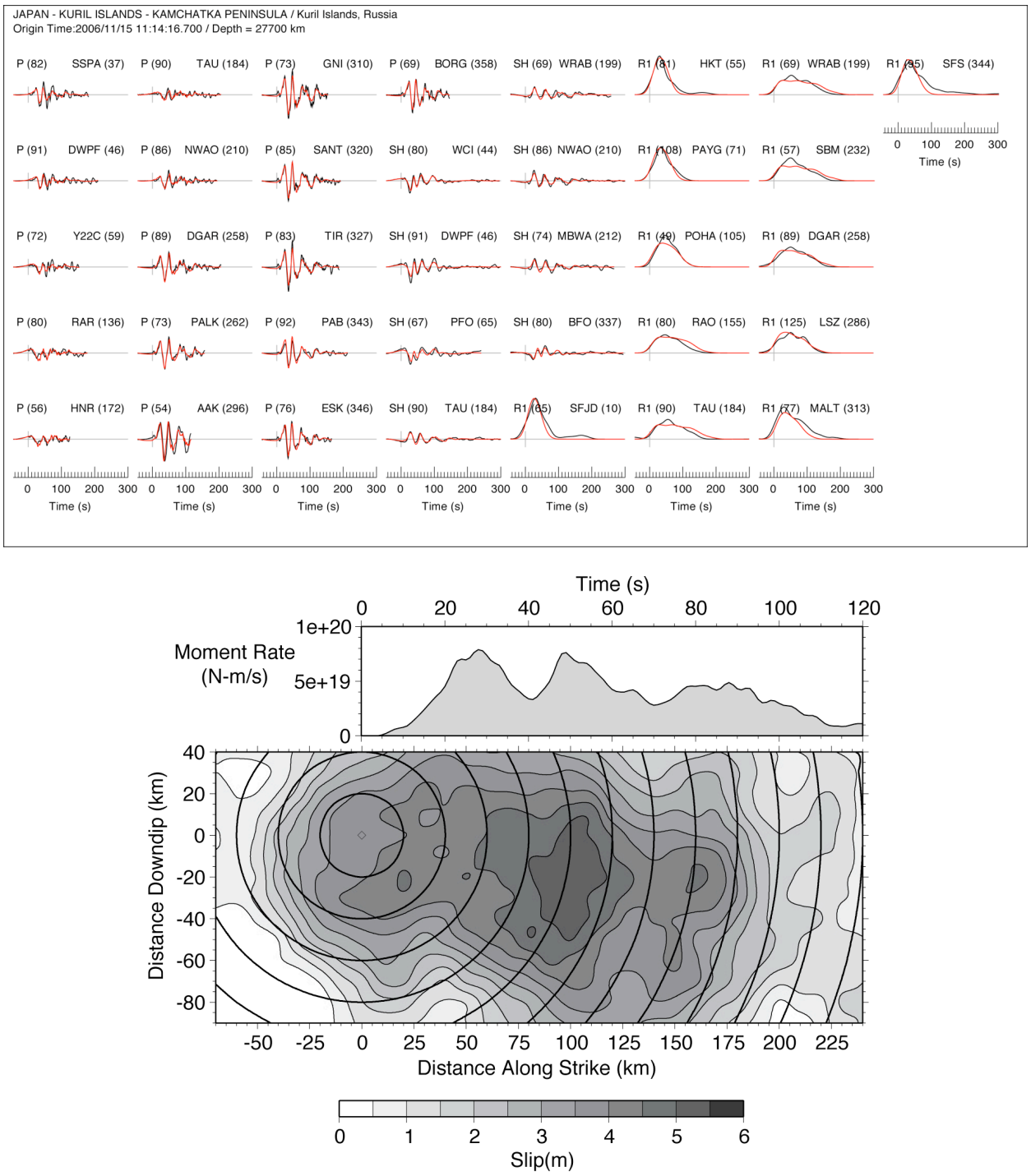

Figure S2 | 15 November 2006 Rupture Model. (Top) Waveform fits for 15 November 2006 for the preferred slip model (Bottom) Data are shown by black lines and model predictions by red lines. Teleseismic P and SH waves resolve shorter scale structure of the source slip function, while dispersion-corrected Rayleigh pulses constrain overall duration and centroid properties of the solution. The source moment rate function is displayed above the slip model with time scale corresponding to the isochrones of the rupture front that spread at 2 km/s.

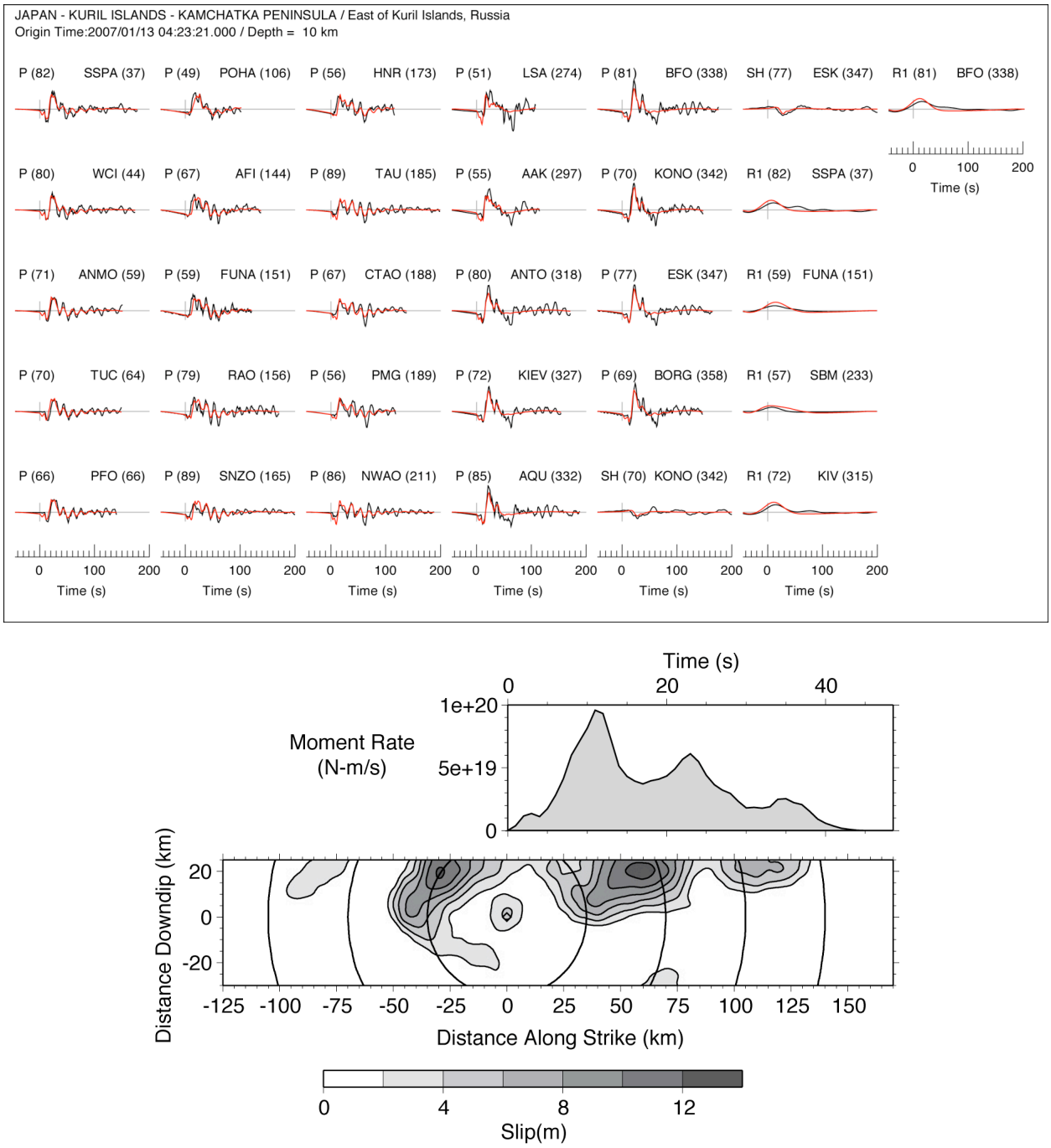

Figure S3 | 13 January 2007 Rupture Model. (Top) Waveform fits for 13 January 2007 for the preferred slip model (Bottom). Data are shown by black lines and model predictions by red lines. Teleseismic P and SH waves resolve shorter scale structure of the source slip function, while dispersion-corrected Rayleigh pulses constrain overall duration and centroid properties of the solution. The source moment rate function is displayed above the slip model with time scale corresponding to the isochrones of the rupture front that spread at 3.5 km/s.

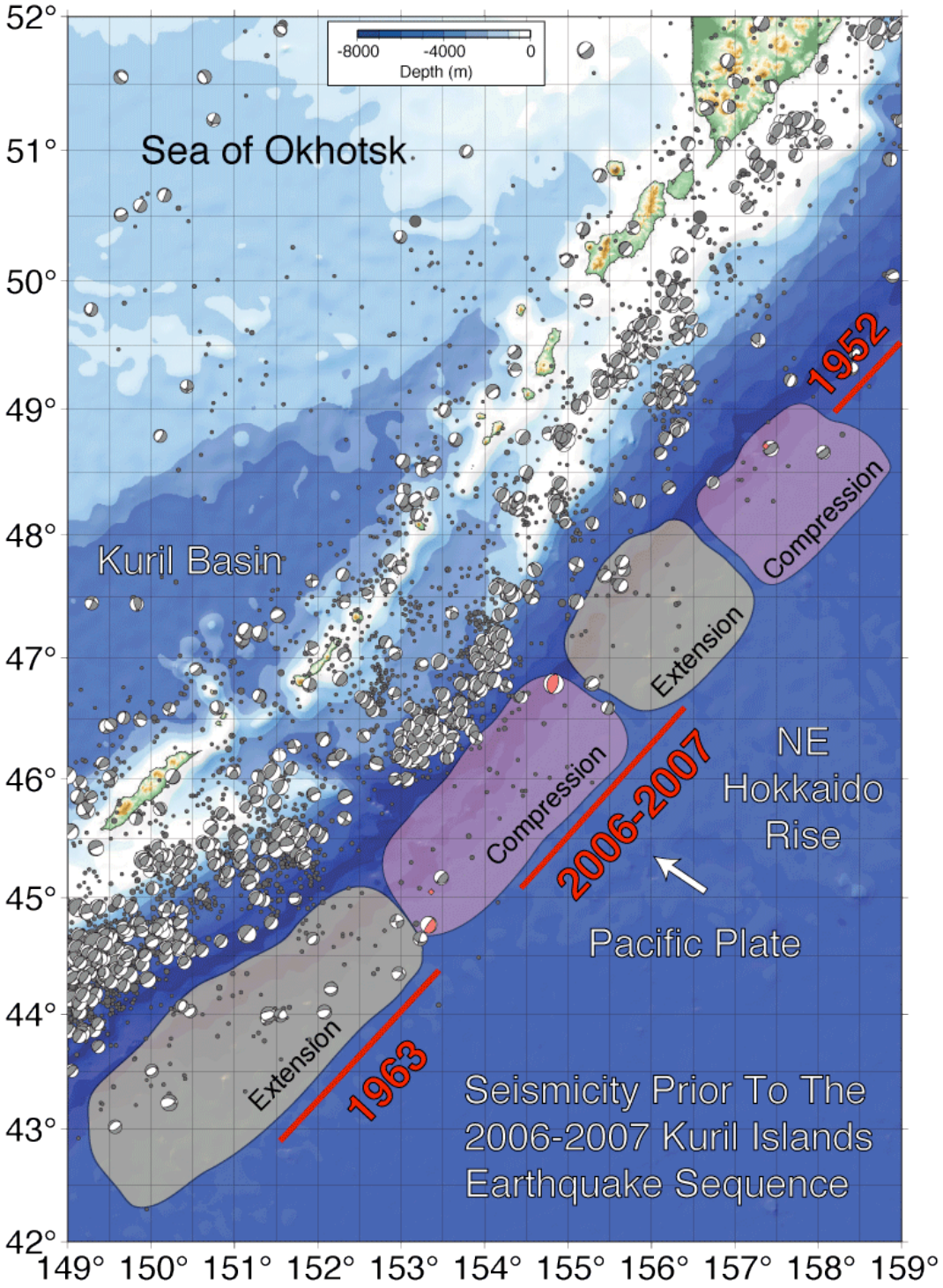

Figure S4 | Regional seismicity. NEIC shallow seismicity distribution and all Harvard centroid-moment tensor solutions for events along the central Kuril Island region prior to the 15 November 2006 event. CMT centroids show an overall bias to the southeast. The compressional focal mechanisms are from (S3). The approximate along-strike lengths of the 1963 Kuril Islands and 1952 Kamchatka earthquakes and the 2006-2007 great doublet are shown by red lines. Outer rise activity of extensional or compressional nature is highlighted.

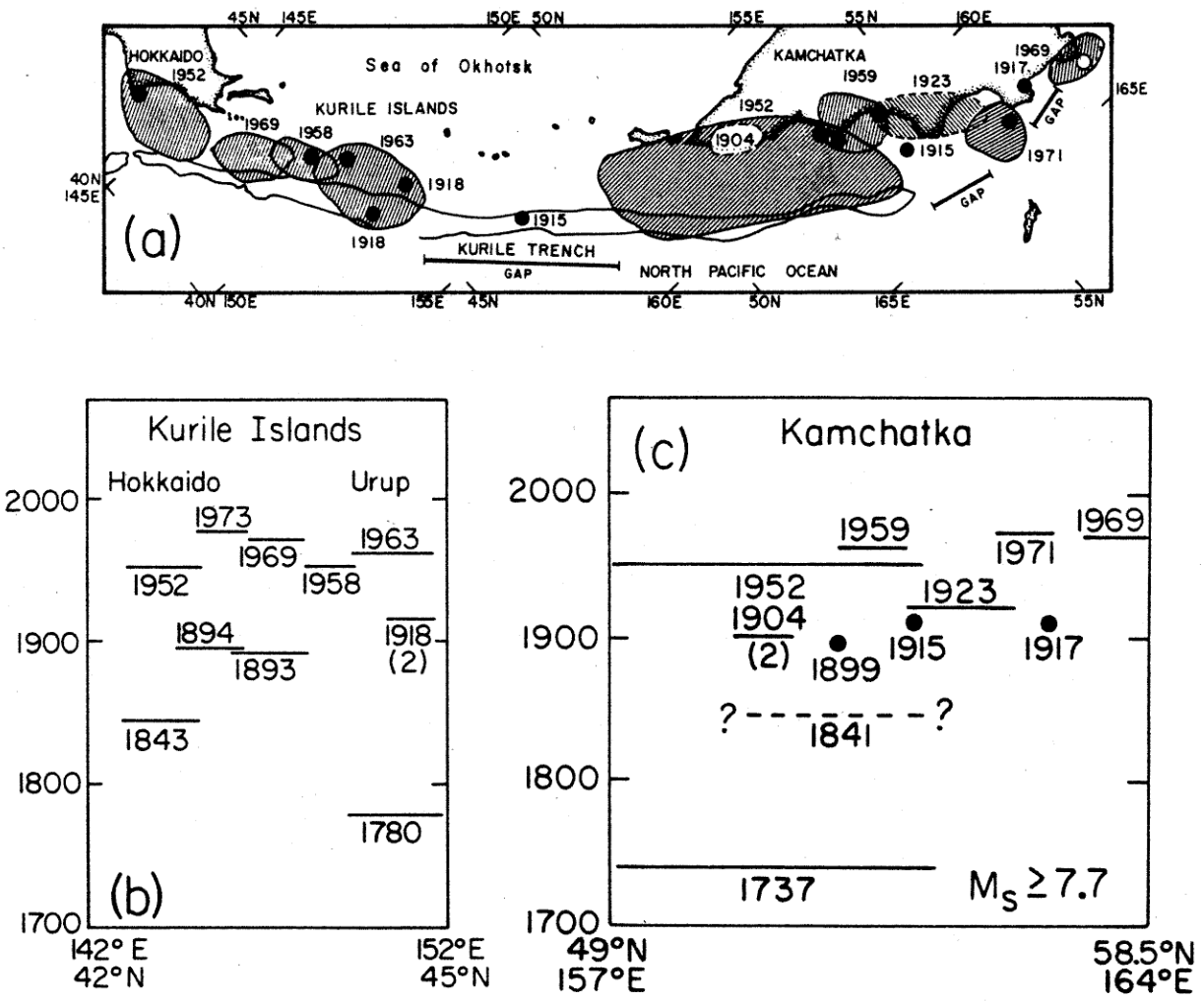

Figure S5 | Historical great earthquakes. Historical record of great earthquakes along the Kuril-Kamchatka arc (S2) indicating locations (a) and time history along the Kuril Islands (b) and Kamchatka peninsula (c). Other than the 1915 event, about which very little is known, there were no large earthquakes in the vicinity of the great doublet in the past century, and this regions was characterized as a seismic gap. Recurrence intervals for great events are about 100 to 200 years along adjacent regions of the megathrust, but the seismic gap had unclear status in terms of being either a region of largely aseismic convergence or a region with potential for large thrust events.

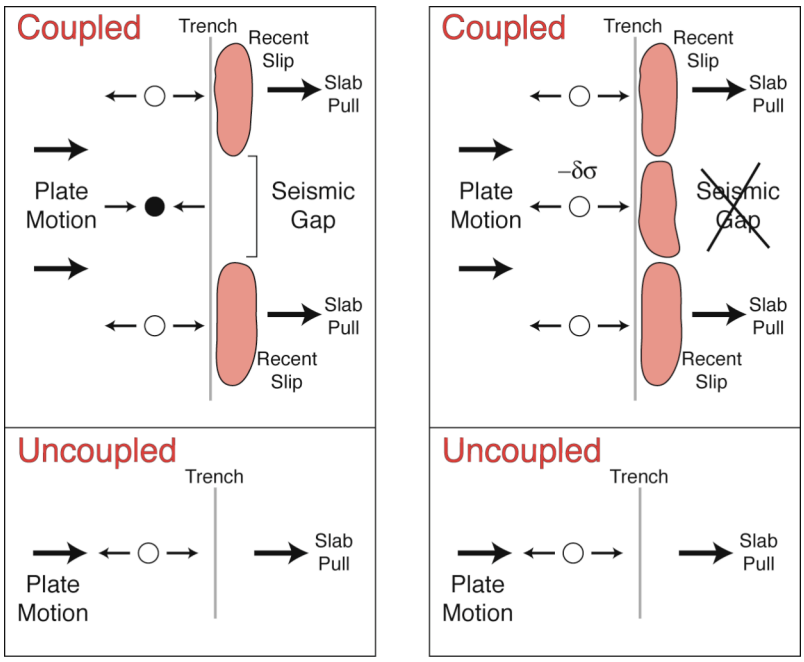

Figure S6 | Outer rise stress modulation model. Conceptual model of how the shallow outer-rise stress environment may be modulated by locking and unlocking of the interplate boundary before and after large thrust earthquakes (S3). For a coupled seismic gap (upper left panel), frictional resistance on the interplate fault raises the neutral surface in the outer rise, enabling shallow outer rise compressional events and reducing the likelihood of outer rise extensional events. When the seismic gap is ruptured (upper right panel), slab pull stresses ($-\delta\sigma$) are communicated to the outer rise, lowering the neutral surface and placing the shallow region of the outer rise in extension, commonly resulting in normal faulting. Outer rise extension due to lithospheric bending/slab pull dominates if there is no seismic coupling on the interplate boundary (lower left and right panels). Any compressional activity in the outer rise should occur at relatively large depths in the latter case.

Supplementary References

S1. http://www.globalcmt.org/CMTsearch.html.

S2. Lay, T., Kanamori, H. & Ruff, L. J. The asperity model and the nature of large subduction zone earthquakes. *Earthquake Prediction Res.* **1,** 3-71 (1982).

S3. Christensen, D. H. & Ruff, L. J. Seismic coupling and outer rise earthquakes. *J. Geophys. Res*. **93**, 13421-13444 (1988).

S4. K. Abe Magnitudes of large shallow earthquakes from 1904 to 1980. *Phys. Earth Planet. Inter.* **27**, 72-92 (1981).